Ain Shams Engineering Journal (2011) 2, 11–20

Ain Shams University

Ain Shams Engineering Journal

www.elsevier.com/locate/asej
www.sciencedirect.com

ELECTRICAL ENGINEERING

A stable adaptive flux observer for a very low speed-sensorless induction motor drives insensitive to stator resistance variations

Mohamed S. Zaky *

Electrical Engineering Department, Faculty of Engineering, Minoufiya University, Egypt

Received 23 December 2010; revised 22 March 2011; accepted 17 April 2011
Available online 1 June 2011

KEYWORDS

Sensorless control;
Stability analysis;
Adaptive law design;
Low speed;
Stator resistance estimation

Abstract In recent years, numerous attempts have been made to improve the performance of sensorless induction motor drives. However, parameter variations, low-speed and zero-speed operations are the most critical aspects affecting the accuracy and stability of sensorless drives. This paper presents a stable adaptive flux observer (AFO) for sensorless induction motor drives insensitive to stator resistance variations. Design of the observer feedback gain of AFO is proposed to guarantee the stability, especially at low speeds. The adaptive law parameters are designed to give quick transient response and good tracking performance. The sensitivity of AFO to stator resistance mismatch is studied. A stator resistance adaptation scheme for accurate speed estimation at low speeds is derived. The relation between the identification error of rotor speed and adaptive gains is clarified based on Lyapunov theory. Experimental setup using DSP-DS1102 control board is implemented. Simulation and experimental results confirm the efficacy of the proposed approach.

1. Introduction

A great interest in the research community is given to develop high performance sensorless induction motor drives. The main approaches to eliminate the speed sensor are based on rotor slot harmonics, frequency signal injection and machine model [1,2]. Speed estimation utilizing rotor slot harmonics have the advantages of being independent of machine parameters. However, they need high precision measurements which increase the hardware/software complexity. Moreover, it may fail for certain slot combinations or skewing. The saliency based technique is machine specific and can not be applied to a standard machine [3]. Methods of speed estimation based on high frequency signal injection in stator voltages or currents

* Tel.: +20 10 8265930; fax: +20 48 2235695.
E-mail address: mszaky78@yahoo.com

Peer review under responsibility of Ain Shams University.
doi:10.1016/j.asej.2011.04.003

Production and hosting by Elsevier

may operate stably under zero-frequency condition, which occurs in regenerative mode at low speeds. However, they may increase losses and introduce torque ripples [1–4].

Machine model based methods of speed estimation have found a great interest among different speed estimation methods for their simplicity. They include different methods such as Model Reference Adaptive System (MRAS) [5]; Kalman Filter (KF) [6]; Adaptive Flux Observer (AFO) [7]; Artificial Intelligence (AI) Techniques [8]; and Sliding Mode Observer (SMO) [9]. Machine model-based methods are characterized by their simplicity and good performance at high and medium speeds. However, at low speeds, they are problematic. The main limitations arise from instability problems associated with most speed estimation schemes at low speeds due to the change of machine parameters. The question that always arises is 'to which extent the method is successful without deteriorating the dynamic performance of the drive during a wide speed range' [1,2].

Adaptive flux observer is one of the machine model based methods of speed estimation of sensorless induction motor drives. Parameter variations, low-speed operation and the difficulty encountered in the design of the feedback gain and the adaptation mechanism are the most critical aspects affecting the accuracy and stability of this method. The characteristics of the speed estimation process are governed by how to deal with the aforementioned issues to guarantee the stability and tracking performance of the speed estimation in the sensorless drives during a wide range [10–20].

Many researches have been devoted to yielding better speed estimation of sensorless induction motor drives using AFO. However, there is a well known unstable region encountered at low speeds. This unstable region of AFO can be reduced by proper design of both the observer feedback gain and adaptive law using several techniques. Instability problems of low speed regenerative mode of reduced-order observers and their remedies have been proposed in [10]. One of the techniques to study the stability analysis of the speed estimation and simplify the structure of the sensorless control system by means of the decoupling control is proposed [11]. Another one utilized Routh–Hurwitz criterion [12]. Others are based on the linearized model of the speed adaptive full-order flux observer [13] or using Lyapunov theory [14]. Alternatively, improving the stability of the AFO by modifying the adaptive law is based on extensive numerical calculation of the current loci, and its stability is analyzed using a two-time-scale approach [15]. The ramp response characteristic of the speed estimator is used as design guidelines for the adaptation gains [14]. Stabilizing MRAS-based estimator for combined speed and stator resistance is achieved by adjusting the adaptive laws [16]. The instability problem for simultaneous estimation of rotor speed and stator resistance using average technique is solved [17]. In [18], all gain selections which give complete stability of AFO are obtained. Stability analysis of both rotor speed and stator resistance estimators for stable AFO in the regenerative mode at low speeds has been presented in [19]. In this work, the observer feedback gain has been designed to guarantee AFO stability. In [20], the reduction of the unstable region in the regenerative mode by an appropriate design of feedback gains and speed adaptation law has been proposed.

Recently, numerous attempts have been made to improve the performance of speed-sensorless induction motor drives, especially at low speeds, by identifying stator resistance together with speed [21–23]. Stator resistance estimation is of utmost importance for accurate operation of sensorless induction motor drives in low speed region and also for minimizing the instability problems associated with AFO in this region. However, little interest has been given for stability analysis of combined speed and stator resistance estimators [13,17,19]. In addition, no criterion clarifies the relation between the adaptive gains and the identification error and how these gains affect both the convergence and steady state error of the speed estimator.

This paper is aimed at developing a stable AFO for speed estimation of sensorless induction motor drives. Design of the observer feedback gain is proposed to guarantee the stability, especially in the low-speed region. The characteristic equation of the closed loop speed estimator is derived. The gains of PI adaptation law are selected based on Root-Locus plot to give fast dynamic response and good tracking performance. The designed AFO is remedied to be insensitive to parameter variations which have a major influence on accuracy and stability of low speed estimation. Therefore, a stator resistance estimation algorithm is used in parallel with rotor speed using Popov's hyper-stability theory. The boundedness of the identification error of the rotor speed and the relation between the identification error and the adaptive gains are clarified using Lyapunov theory. To ensure the validity of the proposed approach, simulation and experimental results are presented at different operating conditions. Good speed estimation compared with actual speed is achieved, especially at very low speeds.

2. Mathematical models for induction motor and adaptive flux observer

2.1. Dynamic model of the induction motor

The induction motor can be described by the following dynamic equations in the synchronous reference frame, using stator current and rotor flux as state variables.

$$p\begin{bmatrix} i_s^e \\ \lambda_r^e \end{bmatrix} = \begin{bmatrix} a_{11} & a_{12} \\ a_{21} & a_{22} \end{bmatrix}\begin{bmatrix} i_s^e \\ \lambda_r^e \end{bmatrix} + \begin{bmatrix} B_{11} \\ 0 \end{bmatrix} v_s^e \tag{1}$$

$$\begin{aligned} \dot{x}^e &= Ax^e + Bv_s^e \\ i_s^e &= Cx^e \end{aligned} \tag{2}$$

where

$$x^e = \begin{bmatrix} i_s^e & \lambda_r^e \end{bmatrix}^{\mathrm{T}},\ i_s^e = \begin{bmatrix} i_{ds}^e & i_{qs}^e \end{bmatrix}^{\mathrm{T}},\ \lambda_r^e = \begin{bmatrix} \lambda_{dr}^e & \lambda_{qr}^e \end{bmatrix}^{\mathrm{T}}$$

The electromechanical equation of the induction motor is given by

$$T_e = \frac{3}{2}\frac{P}{2}\frac{L_m}{L_r}(i_{qs}^e\lambda_{dr}^e - i_{ds}^e\lambda_{qr}^e) \tag{3}$$

2.2. Adaptive flux observer

The adaptive flux observer for estimating stator current and rotor flux can be constructed as follows:

$$\begin{aligned} \hat{\dot{x}}^e &= \hat{A}\hat{x}^e + Bv_s^e + K(\hat{i}_s^e - i_s^e) \\ \hat{i}_s^e &= C\hat{x}^e \end{aligned} \tag{4}$$

where K is the observer gain matrix.

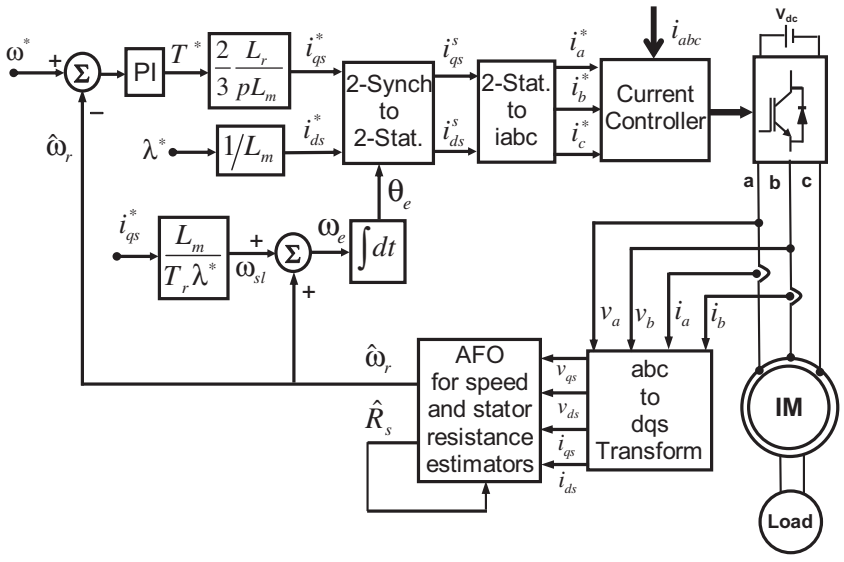

Figure 1 Block diagram of sensorless indirect field oriented control system.

The rotor speed is estimated using the adaptation mechanism similar to the one used in [12]

$$\hat{\omega}_r = K_P \varepsilon + K_I \int \varepsilon \, dt \tag{5}$$

where K_P and K_I are positive adaptation gains and the adaptive error signal ε is [12],

$$\varepsilon = e_{id}\hat{\lambda}_{qr} - e_{iq}\hat{\lambda}_{dr} \tag{6}$$

where

$$e_{id} = \hat{i}_{ds} - i_{ds} \quad \text{and} \quad e_{iq} = \hat{i}_{qs} - i_{qs} \tag{7}$$

To obtain the observer error equation, subtract Eq. (4) from Eq. (2) yielding;

$$\begin{aligned} \dot{e} &= \dot{x}^e - \dot{\hat{x}}^e = (A + KC)e + \Delta A \hat{x}^e \\ e_i &= Ce \end{aligned} \tag{8}$$

The block diagram of the proposed sensorless indirect field oriented (IFO) controlled induction motor drive is shown in Fig. 1.

3. Design of the feedback gain matrix

One of the main problems of designing AFO is determining the observer gain matrix K such that the error dynamics are asymptotically stable with sufficient speed of response. Eq. (8) shows that the dynamic behavior of the error vector is determined by the eigenvalues of the matrix $(A + KC)$. If the matrix $(A + KC)$ is a stable matrix, the error matrix will converge to zero for any initial error vector. If the eigenvalues of the matrix $(A + KC)$ are chosen in such a way that the dynamic behavior of the error vector is asymptotically stable and is adequately fast, the error vector will tend to zero with adequate speed. The first step in the pole placement design approach is to choose the locations of the desired closed loop poles. The most frequently used approach is choosing such poles based on experience in the root locus design, placing a dominant pair of the closed loop poles and choosing other poles so that they are far to the left of the dominant closed loop poles [12,22].

The adaptive flux observer for stator current based on Eq. (4) can be rewritten as,

$$p\hat{i}_s^e = (\hat{a}_{11} + K)\hat{i}_s^e + \hat{a}_{12}\hat{\lambda}_r^e + B_{11}v_s^e - Ki_s^e \tag{9}$$

The observer feedback gain matrix K is given by

$$K = \begin{bmatrix} K_1 & -K_2 \\ K_2 & K_1 \end{bmatrix} \tag{10}$$

$$\hat{a}_{11} + K = \begin{bmatrix} a_1 + K_1 & \omega_e - K_2 \\ -\omega_e + K_2 & a_1 + K_1 \end{bmatrix} \tag{11}$$

The characteristic equation of the AFO is

$$s^2 - 2(a_1 + K_1)s + (a_1 + K_1)^2 + (-\omega_e + K_2)^2 = 0 \tag{12}$$

So, the damping coefficient and the natural frequency can be obtained as follows,

$$\xi = \frac{-(a_1 + K_1)}{\sqrt{(a_1 + K_1)^2 + (-\omega_e + K_2)^2}} \tag{13}$$

$$\omega_n = \sqrt{(a_1 + K_1)^2 + (-\omega_e + K_2)^2} \tag{14}$$

The eigenvalues of the observer are given from Eq. (12) as follows,

$$s_{1,2} = (a_1 + K_1) \pm j(-\omega_e + K_2) \tag{15}$$

These poles should be chosen to obtain robustness and good dynamic performance over a wider range of speed including very low and zero speeds. In practice, the eigenvalues of the observer are designed based on the following principles.

- They have negative real parts to ensure that the system is stable. Also, they are located farther into the left half of the s-plane compared to the eigenvalues of the system, so that the state of the observer converges rapidly.
- In order to increase the observer stability, K_1 should be negative. In other words, the real part of observer poles should be shifted to the left in the s-plane.

- To ensure higher damping of the observer, choose K_1 and K_2 so that the term, $\left|\frac{(-\omega_e+K_2)}{(a_1+K_1)}\right|$, is small in Eq. (13).

Based on the above-mentioned criteria for the pole-placement, the feedback gains are chosen as,

$$K_1 = k_1 a_1, \qquad K_2 = k_2 \omega_r$$

where K_1 is proportional to the induction motor parameters, K_2 is an arbitrary gain and chosen as a function of the rotor speed, k_1 and k_2 are an arbitrary positive constant values.

4. Adaptive law design

To find the values of the PI adaptive gains, we take Laplace transform of Eq. (8):

$$se(s) = (A + KC)e(s) + \Delta A\hat{x}^e \tag{16}$$

$$e(s) = [sI - A - KC]^{-1}\Delta A\hat{x}^e \tag{17}$$

$$e_i(s) = Ce(s) = C[sI - A - KC]^{-1}\Delta A\hat{x}^e \tag{18}$$

The matrix ΔA is expressed as Eq. (19) considering the rotor speed as the only variable parameter,

$$\Delta A = A - \hat{A} = \begin{bmatrix} 0 & n \\ 0 & -1 \end{bmatrix} J\Delta\omega_r \tag{19}$$

$$e_i = C[sI - A - KC]^{-1}\begin{bmatrix} 0 & n \\ 0 & -1 \end{bmatrix} J\Delta\omega_r\hat{x}^e \tag{20}$$

The open loop transfer function between the adaptive error signal and the speed estimation error, assuming the observer gain $K = 0$, is given by Eq. (21). Using Eq. (20) and substituting with the coefficients (A, B, C) one can obtain Eq. (21). All coefficients of Eq. (21) are given in the appendix. The block diagram representing closed loop speed estimator is shown in Fig. 2.

$$G(s) = \frac{\varepsilon}{\Delta\omega_r} = \hat{\lambda}_{ro}^2 \frac{n_o s^3 + n_1 s^2 + n_2 s + n_3}{s^4 + d_1 s^3 + d_2 s^2 + d_3 s + d_4} \tag{21}$$

Fig. 3 shows Root Locus of $G(s)$ at 150 rad/s. As shown, the dominant poles are closer to the imaginary axis, giving slower error reduction. Variation of the dominant poles of $G(s)$ is obtained at different rotor speeds as shown in Fig. 4. The design of K_P and K_I is introduced to ensure stable operation. It can be seen that the design of K_P and K_I is selected to ensure that all of the poles and zeros are located in the left hand side of the s-plane. This allows for the required fast response. The location of the closed-loop transfer function poles characterizes the control system dynamics. Therefore, the location of the PI controller zero should be on the real axis to make sure that the fast dynamic closed-loop poles are always located to the left of the dominant conjugate poles, guaranteeing fast

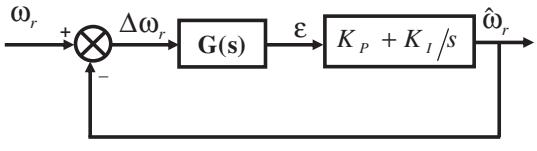

Figure 2 Block diagram representing closed loop speed estimator.

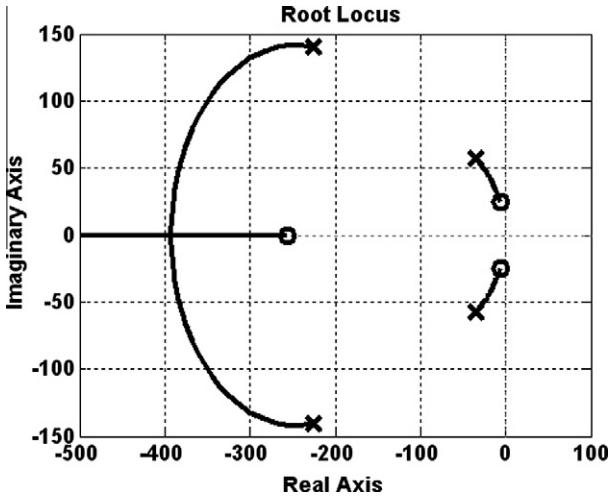

Figure 3 Root Locus showing poles and zeros of $G(s)$ at 150 rad/s.

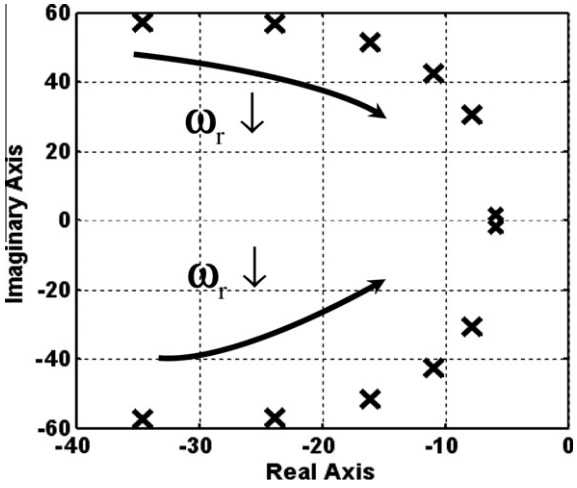

Figure 4 Dominant pole locations of $G(s)$ at different rotor speeds 150, 115, 80, 50, 25 and 2 rad/s.

transient response and good tracking performance. Therefore, K_P is taken of large value and K_I/K_P should equal the negative real part of the dominant poles. This allows for fast exponentially speed error decaying with time without overshoot or undershoot. The location of the PI controller zero K_I/K_P can be selected at any speed from Fig. 4 which shows dominant pole locations of $G(s)$ at different rotor speeds.

5. Sensitivity analysis

Practically, parameter variations are unavoidable due to temperature rise and skin effects. The influence of parameter variations on the speed estimation is investigated by showing how parameter mismatch affects the speed estimation error. The sensitivity to stator resistance variations is firstly studied. Speed estimation error versus the stator resistance mismatch, at different rotor speeds equal to 0.5, 2, 5, and 100 rad/s, is shown in Fig. 5. It can be seen that the speed estimation error dramatically increases at the low speed range. Also, stator resistance variations at high speeds have a very low speed error

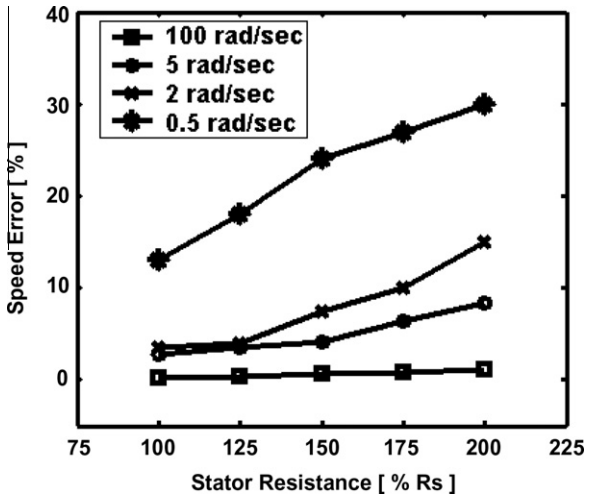

Figure 5 Speed error versus stator resistance variations.

which can not exceed 1.1% at 200% R_s mismatch. On the other hand, the speed estimation error has large values at very low speeds reaching 30% at 200% R_s mismatch. The induced emf in the high speed range is high and the mismatch of the voltage drop across the stator resistance has a negligible effect on the speed estimation. At low speeds, the induced emf is very small and the mismatch of the voltage drop across the stator resistance has a serious influence on the speed estimation, which can lead the system into instability. In order to avoid this, the online stator resistance adaptation scheme has been applied [15,21].

On the other hand, variations of rotor resistance, leakage and mutual inductances do not cause instability problems in the speed estimation as discussed in [14].

6. Speed and stator resistance identification schemes

The aim of this section is to develop AFO which guarantees both stability and convergence of the estimated parameters.

If the rotor speed and stator resistance are considered as variable parameters, assuming no other parameter variations, the matrix ΔA is expressed as follows:

$$\Delta a_{11} = \frac{\Delta R_s I}{L_\sigma},\ \Delta a_{12} = \frac{\Delta \omega_r J}{\varepsilon},\ \Delta a_{21} = 0,\ \Delta a_{22} = -\Delta \omega_r J \quad (22)$$

The error equation of the AFO is given by subtracting Eq. (9) from Eq. (1),

$$\dot{e}_i = a_{11}(\hat{i}_s^e - i_s^e) + (a_{11} - \hat{a}_{11})\hat{i}_s^e + a_{12}(\lambda_r^e - \hat{\lambda}_r^e) + (a_{12} - \hat{a}_{12})\hat{\lambda}_r^e + K(\hat{i}_s^e - i_s^e) \quad (23)$$

The estimation of rotor fluxes is constructed by an open loop observer represented by Eq. (4) without the flux error [22–25], therefore $\lambda_r^e = \hat{\lambda}_r^e$;

Thus the error equation becomes,

$$\dot{e}_i = (a_{11} + K)e_i + \Delta a_{11}\hat{i}_s^e + \Delta a_{12}\hat{\lambda}_r^e \quad (24)$$

6.1. Stability of the identification system

Popov's hyper-stability theory is applied to examine stability of the proposed identification system. This requires that the error system and the feedback system are derived so that the theory could be applied.

In the adaptive observer, using a speed identification error $\Delta\omega_r = \omega_r - \hat{\omega}_r$, a stator resistance identification error $\Delta R_S = R_S - \hat{R}_S$ and an error signal e_i, the error system from Eq. (24) is written as:

$$\dot{e}_i = (a_{11} + K)e_i - W \quad (25)$$

The Popov's integral inequality of Eq. (25) is written as follows [21,22,25]:

$$\int_0^{t_0} e_i^{\mathrm{T}} W \mathrm{d}t \geqslant -\gamma^2, \quad \gamma = \text{const.} \quad (26)$$

where e_i is the input vector and $W = -z_1\Delta R_s - z_2\Delta\omega_r$, which represents the nonlinear block, is the output vector of the feedback block, and is a finite positive constant which does not depend on t_0, and

$$z_1 = (1/L_\sigma)\hat{i}_s^e \quad (27)$$

$$z_2 = (J/\varepsilon)\hat{\lambda}_r^e \quad (28)$$

$$\int_0^t e_i^{\mathrm{T}} W \mathrm{d}t = \int_0^{t0} e_i^{\mathrm{T}}(-z_1\Delta R_s - z_2\Delta\omega_r)\,\mathrm{d}t \quad (29)$$

Substitution of Eqs. (27) and (28) in Eq. (29) yields,

$$\int_0^{t_0}\left(\frac{-e_i^{\mathrm{T}}\Delta R_s}{L_\sigma}\hat{i}_s^e\right)\mathrm{d}t + \int_0^{t_0}\left(\frac{-e_i^{\mathrm{T}}\Delta\omega_r J}{\varepsilon}\hat{\lambda}_r^e\right)\mathrm{d}t \geqslant -\gamma^2 \quad (30)$$

$$\int_0^{t_0}\left(-\frac{e_i^{\mathrm{T}}\Delta R_s}{L_\sigma}\hat{i}_s^e\right)\mathrm{d}t \geqslant -\gamma_1^2 \quad (31)$$

$$\int_0^{t_0}\left(\frac{-e_i^{\mathrm{T}}\Delta\omega_r J}{\varepsilon}\hat{\lambda}_r^e\right)\mathrm{d}t \geqslant -\gamma_2^2 \quad (32)$$

The validity of Popov's inequality of Eq. (26) can be verified by means of the inequalities expressed by Eqs. (31) and (32), provided that the estimates of rotor speed and stator resistance can be obtained by Eqs. (33) and (34), respectively:

$$\hat{\omega}_r = \left(K_{\mathrm{P}\omega} + K_{\mathrm{I}\omega}\int \mathrm{d}t\right)e_i^{\mathrm{T}} J\hat{\lambda}_r^e \quad (33)$$

$$\hat{R}_s = (K_{\mathrm{PR}} + K_{\mathrm{IR}}\int \mathrm{d}t)e_i^{\mathrm{T}}\hat{i}_s^e \quad (34)$$

where $K_{\mathrm{P}\omega}$, $K_{\mathrm{I}\omega}$, K_{PR} and K_{IR} are adaptive gains for speed and stator resistance estimators, respectively.

An identification system for speed and stator resistance is shown in Fig. 6, which is constructed from a linear time-invariant forward block and a nonlinear time-varying feedback block. The system is hyper-stable if the forward block is positive real and the input and output of the nonlinear feedback block satisfy Popov's integral inequality. Block diagram of combined speed and stator resistance estimators is shown in Fig. 7.

6.2. Relation between estimation error and adaptive gains

This section will show the boundedness of the identification error of the rotor speed when the rotor speed is time-varying, and clarify the relation between the identification error and

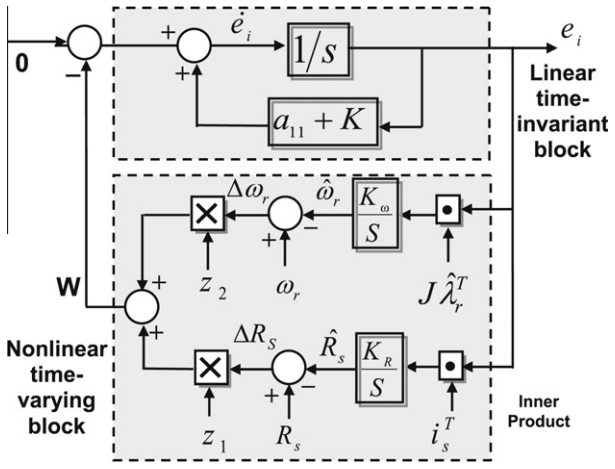

Figure 6 Block diagram represented speed and stator resistance identification system.

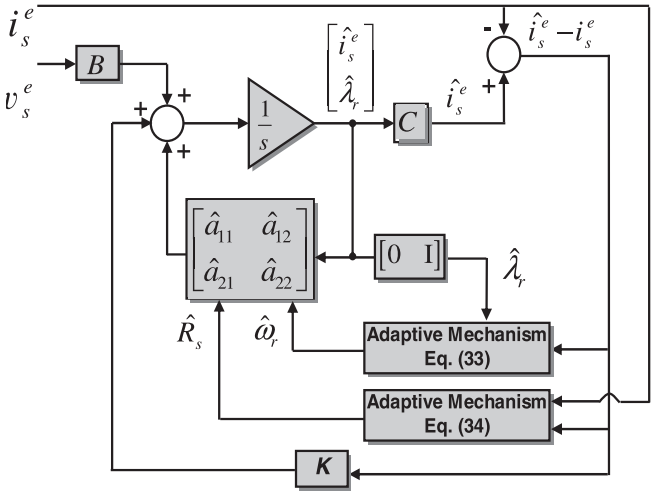

Figure 7 Block diagram of combined speed and stator resistance estimation.

the adaptive gains. Considering the block diagram of Fig. 2 yields,

$$\hat{\omega}_r = \left(K_{P\omega} + \frac{K_{I\omega}}{s}\right) G(s)\Delta\omega_r \tag{35}$$

from which;

$$\Delta\dot{\omega}_r = -\frac{K_{I\omega}\cdot G(s)|_{s=0}}{1+K_{P\omega}\cdot G(s)|_{s=0}}\Delta\omega_r + \frac{1}{1+K_{P\omega}\cdot G(s)|_{s=0}}\dot{\omega}_r \tag{36}$$

Now let the following conditions be satisfied:

$$\frac{K_{I\omega}\cdot G(s)|_{s=0}}{1+K_{P\omega}\cdot G(s)|_{s=0}} > 0 \tag{37}$$

$$|\dot{\omega}_r| < \mu \text{ (const.)} \tag{38}$$

The condition in Eq. (37) is the necessary condition for the stability of the identifier which must always be satisfied. However, the condition in Eq. (38) is the natural condition on the bound of the acceleration/deceleration determined by the mechanical load conditions.

The Lyapunov function must be determined in order to illustrate the relation between the estimation error and adaptive gains according to the Lyapunov stability theory.

The Lyapunov function V is chosen as;

$$V = \frac{1}{2}\Delta\omega_r^2 \tag{39}$$

The time derivative of V can be expressed as;

$$\dot{V} = \Delta\omega_r \cdot \Delta\dot{\omega}_r \tag{40}$$

According to Lyapunov stability theory, a system is stable when a positive definite Lyapunov function has a negative definite first derivative. The condition of Eq. (40) being negative definite will be satisfied if $\dot{V} < 0$.

$$\dot{V} = -\frac{K_{I\omega}\cdot G(s)|_{s=0}}{1+K_{P\omega}\cdot G(s)|_{s=0}}|\Delta\omega_r|[|\Delta\omega_r| - d_{\max}] < 0 \tag{41}$$

$$|\Delta\omega_r| < d_{\max} \tag{42}$$

where;

$$d_{\max} = \frac{\mu}{K_{I\omega}\cdot G(s)|_{s=0}} \tag{43}$$

From the aforementioned results, it is clear that the bound of the identification error in Eq. (43) is determined only by the integral gain $K_{I\omega}$ and is independent of the proportional gain $K_{P\omega}$. The proportional gain $K_{P\omega}$ contributes to the enhancement of the rate of convergence. This analysis is proved by Fig. 8 which shows the reference, actual and estimated speeds and speed estimation error during a step change of speed from 10 to 100 rad/s at different adaptive gain values. As shown in the figure, the speed estimation error increases with decreasing the integral gain $K_{I\omega}$. The results show how the choice of the correct values of PI adaptation gains affects the convergence of the estimated speed to the actual one. Simulation results in the regenerative mode at low speeds with and without the feedback gain are shown in Fig. 9. This figure demonstrates the instability phenomenon of AFO without feedback gain and its remedy with the proposed feedback gain. These results are taken at 5 rad/s and $T_L = -2$ N m.

7. Results and discussions

The proposed algorithms of speed and stator resistance estimators are developed on a DSP-DS1102 control board. The main processing unit on the DS1102 control board is a Texas Instrument TMS320C31 DSP with 60 MHz system clock. This control board is hosted by a personal computer for processing and downloading the control programs. The speed-sensorless control system is shown in Fig. 1. The motor is driven by the sensorless controller, with the estimated speed fed back for the speed loop control. All the variables in the observer and controller are initialized to zeros before running the drive. Also, all system parameters are first downloaded. The startup procedure is started by the acceleration to the commanded speed.

The experimental system, shown in Fig. 10, is built in laboratory to verify the accuracy of speed estimation based on AFO with stator resistance adaptation scheme. The parameters of the induction motor used as well as the speed controller gains and adaptive PI gains of speed and stator resistance estimators are given in Tables 1–3, respectively. Experimental results are presented to investigate the stability of the drive

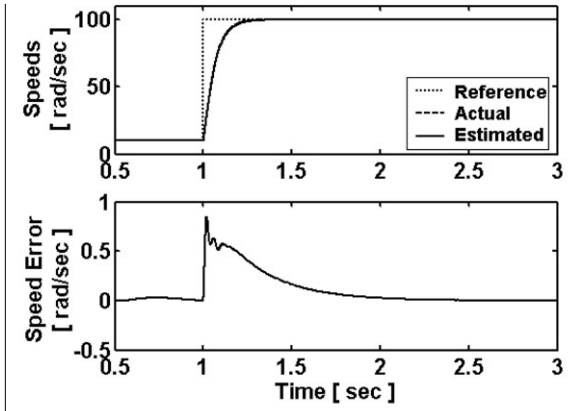

(a) $K_I = 2000$ and $K_P = 550$

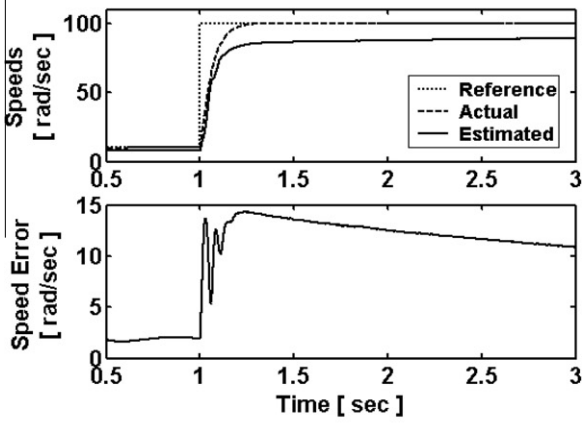

(b) $K_I = 20$ and $K_P = 550$

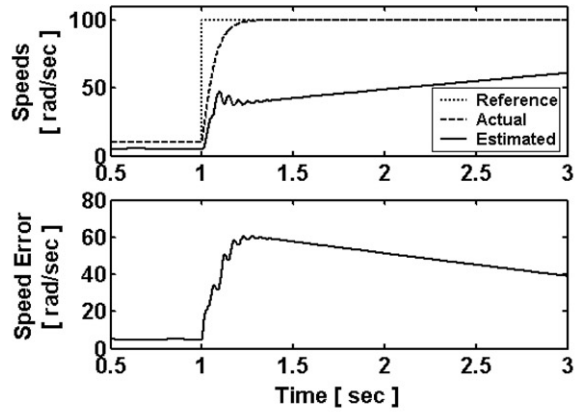

(c) $K_I = 5$ and $K_P = 550$

Figure 8 Reference, actual and estimated speeds and speed estimation error during step change of speed reference from 10 to 100 rad/s at different values of PI gains (Simulation).

system at low speed operation. In addition the robustness of AFO to stator resistance mismatch and load torque disturbances is also investigated. Fig. 11 shows the estimated speed during zero speed operation with initial $+20\%$ R_s mismatch in the speed observer under light load of 20% of the rated value (2 N m). As shown, there exists a substantial speed estimation error. Activation of stator resistance adaptation scheme is turned on at $t = 3$ s. It is clear that the stator resistance estimator quickly removes the initial stator resistance error and consequently, eliminates the large speed estimation error. A considerable reduction of the speed error is observed with stator resistance adaptation due to $+20\%$ initial R_s mismatch in the observer.

The drive system is also tested during dynamic performance. Figs. 12 and 13 show the reference, actual and estimated speeds during very low speed reversal from 3 to -3 rad/s and from 1 to -1 rad/s, respectively under constant load of approximately 50% of the rated value. As shown, a good agreement between the actual and estimated speeds is achieved.

Fig. 14 shows the reference, actual and estimated speeds during zero speed operation with a sudden load change from light load (20%) to the rated value. It is obvious that the estimated speed tracks correctly the actual one. This confirms the robustness of the speed observer to load disturbances. The rotor speed and stator resistance are estimated by stable observers, therefore the proposed observers confront no problem in the low speed region. Furthermore, the algorithms of parallel speed and stator resistance identification scheme are characterized by their simplicity and small computation time.

Simulation and experimental results prove the ability of the AFO to provide an accurate speed estimate in the very low speed region. Moreover, the designed AFO is insensitive to stator resistance variations and is robust to a sudden load change.

8. Conclusion

A design strategy for both feedback gain and adaptation gains of AFO, to guarantee the stability and tracking performance of the speed estimation in the sensorless drives, has been presented. The values of the adaptive law parameters have been determined using Root-Locus plot. The rotor speed and stator resistance have been estimated by stable observers; therefore, they give good operation in the low speed region. It has been made obvious that the bound of the identification error has been determined only by the integral gain and is independent of the proportional gain. The proportional gain contributes to the enhancement of the rate of convergence. The drive system has been tested during different operating conditions including dynamic performance and zero speed operation. Very low speed sensorless operation and also zero speed have been investigated by the proposed AFO with online stator resistance adaptation scheme without losing stability. Simulation and experimental results prove the ability of the AFO to provide an accurate speed estimate in the very low speed region. Moreover, the designed AFO is insensitive to stator resistance variations and is robust to a sudden load change. The results confirm the efficacy and the validity of the proposed approach for sensorless induction motor drives.

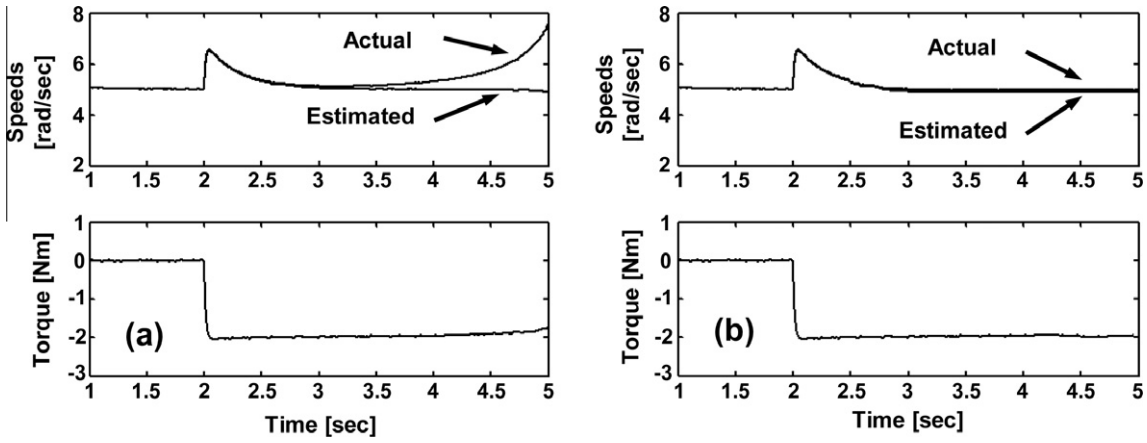

Figure 9 Simulation results during low speed regenerative operation at 5 rad/s and $T_L = -2$ N m. (a) The instability problem with $K = 0$, (b) elimination of the instability problem with the proposed K.

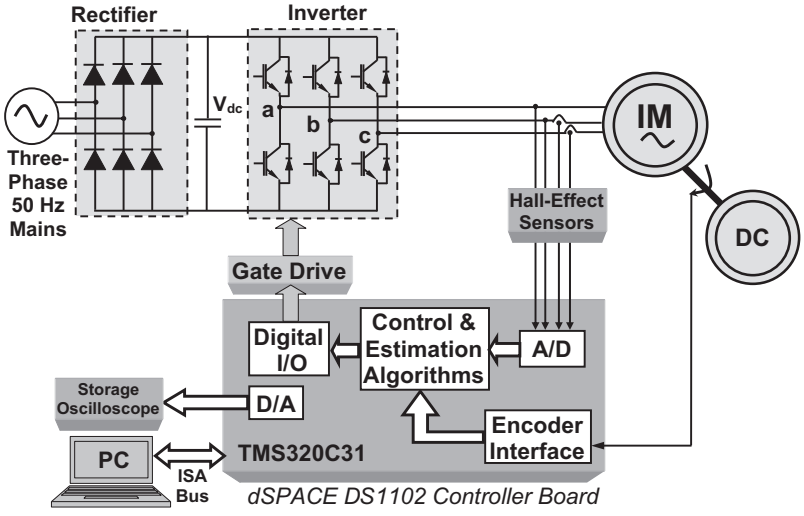

Figure 10 The sensorless control system of the induction motor drive using DSP-DS1102 board.

Appendix A

A.1. List of symbols

L_m	Magnetizing inductance
L_s, L_r	Stator and rotor self inductances
R_s	Stator resistance
T_r	Rotor time constant
ω_r, $\hat{\omega}_r$	Actual and estimated rotor speeds
L_σ	Leakage coefficient
$i_s^e = [i_{ds}^e i_{qs}^e]^T$, $\hat{i}_s^e = [\hat{i}_{ds}^e \hat{i}_{qs}^e]^T$	Actual and estimated stator current vectors
$\lambda_r^e = [\lambda_{dr}^e \lambda_{qr}^e]^T$, $\hat{\lambda}_r^e = [\hat{\lambda}_{dr}^e \hat{\lambda}_{qr}^e]^T$	Actual and estimated rotor flux vectors
$v_s^e = [v_{ds}^e v_{qs}^e]^T$	Stator voltage vector

Table 1 Induction motor parameters.

Rated power (W)	250	R_s (Ω)	7.4826
Rated voltage (V)	380	R_r (Ω)	3.6840
Rated current (A)	1.5	L_s (H)	0.4335
Rated speed (rpm)	1400	L_r (H)	0.4335
Rated frequency (Hz)	50	L_m (H)	0.4114
Number of poles	4	Torque (N m)	2
Moment of Inertia J (kg m^2)	0.0007		

Table 2 Controller parameters.

Speed controller	
Proportional gain	0.7
Integral gain	0.01

Table 3 Adaptive PI gains of speed and stator resistance estimators.

Speed estimator	$K_{P\omega}$	550
	$K_{I\omega}$	2000
Stator resistance estimator	K_{PR}	300
	K_{IR}	1500

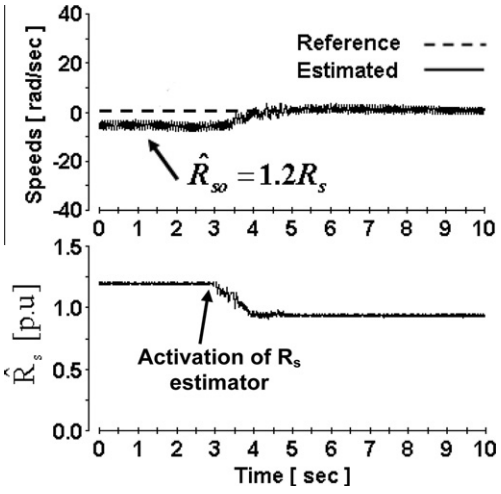

Figure 11 Reference and estimated speeds during zero speed operation with +20% R_s mismatch under constant load of 20% of the rated value. Stator resistance adaptation is activated at $t = 3$ s (Experimental).

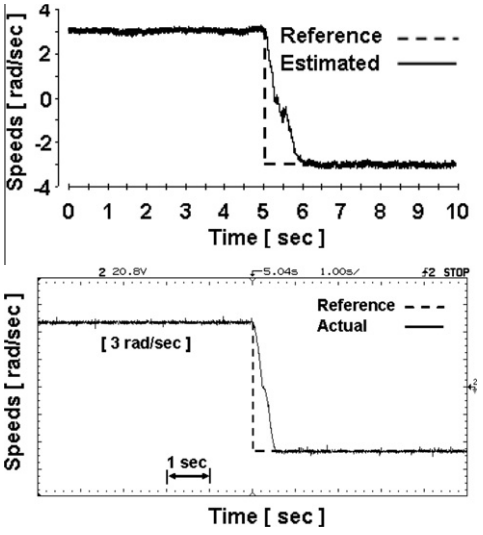

Figure 12 Reference, actual and estimated speeds during speed reversal at 3 rad/s with stator resistance adaptation under constant load of 50% of the rated value (Experimental).

A.2. Induction motor model

The induction motor model in synchronous reference frame in terms of stator currents and rotor fluxes can be written as;

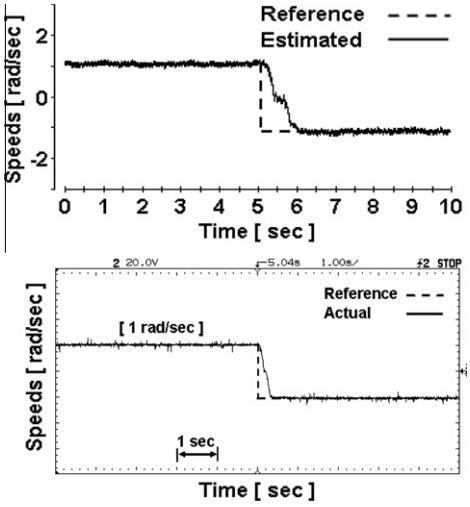

Figure 13 Reference, actual and estimated speeds during speed reversal at 1 rad/s with stator resistance adaptation under constant load of 50% of the rated value (Experimental).

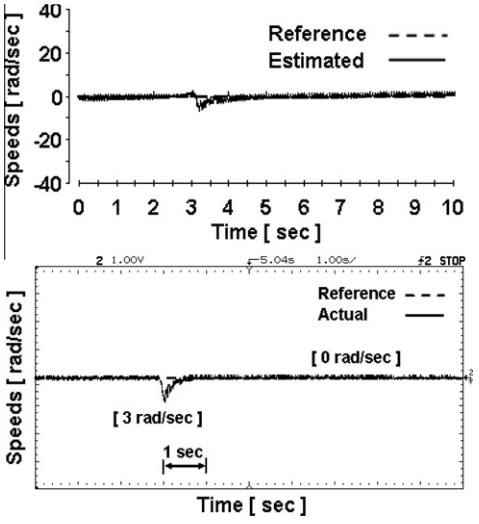

Figure 14 Reference, actual and estimated speeds during zero speed operation with stator resistance adaptation under a sudden load change from 20% to the rated value at $t = 3$ s (Experimental).

$$pi_{ds}^e = a_1 i_{ds}^e + \omega_e i_{qs}^e + a_2 \lambda_{dr}^e + a_3 \lambda_{qr}^e + b v_{ds}^e$$
$$pi_{qs}^e = a_1 i_{qs}^e - \omega_e i_{ds}^e + a_2 \lambda_{qr}^e + a_3 \lambda_{dr}^e + b v_{qs}^e$$

$$p\lambda_{qr}^e = -\omega_s \lambda_{dr}^e + a_5 \lambda_{qr}^e + a_4 i_{qs}^e$$
$$p\lambda_{dr}^e = \omega_s \lambda_{qr}^e + a_5 \lambda_{dr}^e + a_4 i_{ds}^e$$

$$I = \begin{bmatrix} 1 & 0 \\ 0 & 1 \end{bmatrix}, \quad J = \begin{bmatrix} 0 & -1 \\ 1 & 0 \end{bmatrix}$$

$$a_{11} = a_1 I - \omega_e J, \quad a_{12} = a_2 I + a_3 J, \quad a_{21} = a_4 I,$$
$$a_{22} = a_5 I + \omega_s J, \quad \omega_s = \omega_e - \omega_r$$

$$a_1 = -\left(\frac{R_s}{L_\sigma} + \frac{L_m^2}{L_r T_r L_\sigma}\right),\quad a_2 = \frac{L_m}{L_r T_r L_\sigma},\quad a_3 = \frac{L_m}{L_r L_\sigma}\omega_r$$

$$a_4 = \frac{L_m}{T_r},\quad a_5 = \frac{-1}{T_r},\quad B_{11} = bI,\quad b = \frac{1}{L_\sigma},\quad C = [I \quad 0]$$

$$L_\sigma = L_s - \frac{L_m^2}{L_r},\quad T_r = \frac{L_r}{R_r},\quad \varepsilon = \frac{L_m}{L_r T_r L_\sigma},\quad n = \frac{L_m}{L_r L_\sigma}$$

A.3. Coefficients of G(s) are

$$n_o = n$$
$$n_1 = na_1 + 2na_5 - a_2$$
$$n_2 = -na_5^2 - n\omega_s^2 - 2na_1a_5 + na_2a_4 + a_3\omega_s + a_2a_5 + a_1a_2 - a_3\omega_e$$
$$n_3 = na_1a_5^2 + na_1\omega_s^2 - na_2a_4a_5 + na_3a_4\omega_s - a_1a_3\omega_s - a_1a_2a_5 - a_2\omega_e\omega_s + a_3a_5\omega_e + a_4a_2^2 + a_4a_3^2$$
$$d_1 = -(2a_1 + 2a_5)$$
$$d_2 = a_1^2 + a_5^2 + \omega_s^2 + \omega_e^2 + 4a_1a_5 - 2a_2a_4$$
$$d_3 = 2a_2a_4a_5 + 2a_3a_4\omega_s - 2a_1a_5^2 - 2a_1\omega_s^2 - 2a_1^2a_5 + 2a_1a_2a_4 - 2a_5\omega_e^2 - 2a_3a_4\omega_e$$
$$d_4 = -2a_1a_2a_4a_5 - 2a_1a_3a_4\omega_s + a_1^2a_5^2 + a_1^2\omega_s^2 - 2a_2a_4\omega_e\omega_s + 2a_3a_4a_5\omega_e + \omega_e^2a_5^2 + \omega_s^2\omega_e^2 + a_4^2a_2^2 + a_4^2a_3^2$$

References

[1] Zaky M, Khater M, Yasin H, Shokralla SS. Review of different speed estimation schemes for sensorless induction motor drives. J Elect Eng 2008;8(2):102–40.

[2] Holtz J. Sensorless control of induction motor drives. IEEE Proc 2002;90(8):1359–94.

[3] Staines SC, Caruana C, Asher MG, Sumner M. Sensorless control of induction machines at zero and low frequency using zero sequence currents. IEEE Trans Ind Electron 2006;53(1):195–206.

[4] Hinkkanen M, Leppanen VM, Luomi J. Flux observer enhanced with low-frequency signal injection allowing sensorless zero-frequency operation of induction motors. IEEE Trans Ind Appl 2005;41(1):52–9.

[5] Kowalska TO, Dybkowski M. Stator-current-based MRAS estimator for a wide range speed-sensorless induction-motor drive. IEEE Trans Ind Electron 2010;57(4):1296–308.

[6] Marei MI, El-Sattar AA, Mahmoud EA. Reduced order models for speed estimation of sensorless induction motor drives based on Kalman Filter and RLS Algorithm. Int J Eng Intell Syst 2010;18(1):25–33.

[7] Kubota H, Matsuse K, Nakano T. DSP-based speed adaptive flux observer of induction motor. IEEE Trans Ind Appl 1993;29(2):344–8.

[8] Gadoue SM, Giaouris D, Finch JW. Sensorless control of induction motor drives at very low and zero speeds using neural network flux observer. IEEE Trans Ind Electron 2009;56(8):3029–39.

[9] Zaky M, Khater M, Yasin H, Shokralla SS. Very low-speed and zero speed estimation of sensorless induction motor drives. Elect Power Syst Res (EPSR) J 2010;80(2):143–51.

[10] Harnefors L. Instability phenomena and remedies in sensorless indirect field oriented control. IEEE Trans Power Electron 2000;15(4):733–43.

[11] Suwankawin S, Sangwongwanich S. A speed-sensorless IM drive with decoupling control and stability analysis of speed estimation. IEEE Trans Ind Electron 2002;49(2):444–55.

[12] Kubota H, Sato I, Tamura Y, Matsuse K, Ohta H, Hori Y. Regenerating-mode low-speed operation of sensorless induction motor drive with adaptive observer. IEEE Trans Ind Appl 2002;38(4):1081–6.

[13] Hinkkanen M. Analysis and design of full-order flux observers for sensorless induction motors. IEEE Tran Ind Electron 2004;51(5):1033–40.

[14] Suwankawin S, Sangwongwanich S. Design strategy of an adaptive full-order observer for speed-sensorless induction-motor drives-tracking performance and stabilization. IEEE Trans Ind Electron 2006;53(1):96–119.

[15] Tajima H, Guidi G, Umida H. Consideration about problems and solutions of speed estimation method and parameter tuning for speed-sensorless vector control of induction motor drives. IEEE Trans Ind Appl 2002;38(5):1282–9.

[16] Rashed M, Stronach FA. A Stable back-emf MRAS-based sensorless low speed induction motor drive insensitive to stator resistance variation. IEE Proc Electr Power Appl 2004;151(6):685–93.

[17] Saejia M, Sangwongwanich S. Averaging analysis approach for stability analysis of speed-sensorless induction motor drives with stator resistance estimation. IEEE Trans Ind Electron 2006;53(1):162–77.

[18] Harnefors L, Hinkkanen M. Complete stability of reduced-order and full-order observers for sensorless IM drives. IEEE Trans Ind Electron 2008;55(3):1319–29.

[19] Zaky MS. Stability analysis of simultaneous estimation of speed and stator resistance for speed-sensorless induction motor drives. In: Proceedings of 13th International Middle-East Power Systems Conference (MEPCON'2010), Cairo University, Egypt, 2010. p. 364–70.

[20] Etien E, Chaigne C, Bensiali N. On the stability of full adaptive observer for induction motor in regenerating mode. IEEE Trans Ind Electron 2010;57(5):1599–608.

[21] Zaky MS, Khater MM, Yasin HA, Shokralla SS. Wide Speed range estimation with online parameter identification schemes of sensorless induction motor drives. IEEE Trans Ind Electron 2009;56(5):1699–707.

[22] Kojabadi MH, Chang L, Doraiswami R. A MRAS-based adaptive pseudo-reduced-order flux observer for sensorless induction motor drives. IEEE Trans Power Electron 2005;20(4):930–8.

[23] Kojabadi HM, Chang L, Doraiswami R. Novel adaptive observer for very fast estimation of stator resistance in sensorless induction motor drives. In: Proc IEEE Power Electronics Specialist Conf (PESC'03), 2003. p. 1455–9.

[24] Lin YN, Chen CL. Adaptive pseudoreduced-order flux observer for speed sensorless field oriented control of IM. IEEE Trans Ind Electron 1999;46(5):1042–5.

[25] Kojabadi HM, Chang L. Model reference adaptive system pseudo reduced-order flux observer for very low and zero speeds estimation in sensorless induction motors drives. In: Proceedings of IEEE Power Electronics Specialists Conference (PESC'02), 2002. p. 301–8.

Mohamed S. Zaky was born in Minoufiya, Egypt, on January 11, 1978. He received the B.Sc. (with first-class honors), M.Sc., and Ph.D. degrees in Electrical Engineering from Minoufiya University, Shebin El-Kom, Egypt, in 2001, 2005, and 2008, respectively. In 2002, he became an Instructor with Minoufiya University, and then was an Assistant Lecturer in 2006. In 2008 till now, he became lecturer with the Department of Electrical Engineering, Faculty of Engineering; Minoufiya University. His research interests include control of electrical machines; applications of power electronics, DSP-based real time control and renewable energy.